THE JOURNAL OF PHYSICAL CHEMISTRY B

Article

Cite This: J. Phys. Chem. B 2019, 123, 5048−5058

pubs.acs.org/JPCB

Dynamic Nuclear Polarization Magic-Angle Spinning Nuclear Magnetic Resonance Combined with Molecular Dynamics Simulations Permits Detection of Order and Disorder in Viral Assemblies

Rupal Gupta,[‡,∥,#] Huilan Zhang,[‡,∥] Manman Lu,[‡,∥] Guangjin Hou,[‡,∥,●] Marc Caporini,[§,†] Melanie Rosay,[§] Werner Maas,[§] Jochem Struppe,[§] Jinwoo Ahn,[∥,▽] In-Ja L. Byeon,[∥,▽] Hartmut Oschkinat,[○] Kristaps Jaudzems,[◆] Emeline Barbet-Massin,[◆] Lyndon Emsley,[¶] Guido Pintacuda,[*,◆] Anne Lesage,[*,◆] Angela M. Gronenborn,[*,∥,▽] and Tatyana Polenova[*,‡,∥]

[‡]Department of Chemistry and Biochemistry, University of Delaware, Newark, Delaware 19716, United States

[§]Bruker Biospin Corporation, 15 Fortune Drive, Billerica, Massachusetts 01821, United States

[∥]Pittsburgh Center for HIV Protein Interactions and [▽]Department of Structural Biology, University of Pittsburgh School of Medicine, 3501 Fifth Avenue, Pittsburgh, Pennsylvania 15213, United States

[○]Leibniz-Institut für Molekulare Pharmakologie, Robert-Roessle-Str. 10, 13125 Berlin, Germany

[◆]Centre de RMN à Très Hauts Champs, Institut des Sciences Analytiques, UMR 5280 CNRS / Ecole Normale Supérieure de Lyon, 5 Rue de la Doua, Villeurbanne, 69100 Lyon, France

[¶]Institut des Sciences et Ingénierie Chimques, Ecole Polytechnique Fédérale de Lausanne (EPFL) CH-1015 Lausanne, Switzerland

Supporting Information

ABSTRACT: We report dynamic nuclear polarization (DNP)-enhanced magic-angle spinning (MAS) NMR spectroscopy in viral capsids from HIV-1 and bacteriophage AP205. Viruses regulate their life cycles and infectivity through modulation of their structures and dynamics. While static structures of capsids from several viruses are now accessible with near-atomic-level resolution, atomic-level understanding of functionally important motions in assembled capsids is lacking. We observed up to 64-fold signal enhancements by DNP, which permitted in-depth analysis of these assemblies. For the HIV-1 CA assemblies, a remarkably high spectral resolution in the 3D and 2D heteronuclear data sets permitted the assignment of a significant fraction of backbone and side-chain resonances. Using an integrated DNP MAS NMR and molecular dynamics (MD) simulation approach, the conformational space sampled by the assembled capsid at cryogenic temperatures was mapped. Qualitatively, a remarkable agreement was observed for the experimental $^{13}C/^{15}N$ chemical shift distributions and those calculated from substructures along the MD trajectory. Residues that are mobile at physiological temperatures are frozen out in multiple conformers at cryogenic conditions, resulting in broad experimental and calculated chemical shift distributions. Overall, our results suggest that DNP MAS NMR measurements in combination with MD simulations facilitate a thorough understanding of the dynamic signatures of viral capsids.

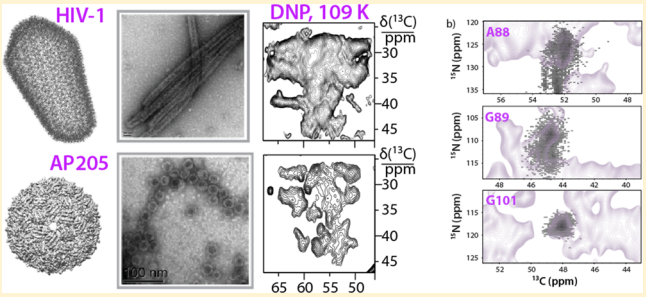

INTRODUCTION

Biological function is invariably connected to and depends on the structure and dynamics of biological macromolecules and their complexes. Nuclear magnetic resonance (NMR) is one of the most powerful techniques to elucidate the intricate relationship between conformational flexibility and function as, in contrast to X-ray diffraction and cryo-EM, it yields atomic-level information on both well-structured and dynamically disordered regions of individual biomolecules and assemblies. NMR experiments provide direct access to a number of site-specific experimental parameters (chemical shifts, residual anisotropic interactions, and relaxation rates) that report directly on both structure and dynamics. These studies can be performed in solution on relatively small or flexible components or on microcrystalline or sedimented assemblies under magic-angle spinning (MAS) conditions.[1−13]

Typically, NMR experiments conducted at noncryogenic temperatures provide dynamics information from averaged

Received: March 11, 2019
Revised: May 22, 2019
Published: May 24, 2019

DOI: 10.1021/acs.jpcb.9b02293
J. Phys. Chem. B 2019, 123, 5048−5058

observables, reflecting the state of an ensemble of conformers, all of which contribute to the observable in a weighted manner. Solution NMR methods for studying dynamics are advanced, and ensemble analyses have been developed to describe the conformational space and the timescale of the interconversions.[14−17] Extensive site-specific studies of dynamics in proteins and protein assemblies by solid-state NMR still remain relatively rare and challenging, often suffering from low sensitivity. The most commonly used approaches rely on the measurement of various relaxation rates and their temperature dependencies,[18−20] relaxation dispersion curves,[21,22] dipolar and/or chemical shift anisotropy tensors,[2,8,13] and a combination of these methods.[23] These techniques yield information on motional rates and/or amplitudes and symmetries over a broad range of timescales (see a recent review[24]).

One example where motions are important in the regulation of biological function is virus capsids,[25] where dynamic regulation emerges as a key feature of assembly and disassembly and of genome encapsidation. Local dynamics have been observed in large ordered assemblies, and some viral capsids contain both ordered and disordered structural elements.[13,26] Numerous recent solution NMR studies have described conformational disorder in viral proteins alone or in complexes, such as paramyxoviral phosphoproteins, nucleoproteins, and HIV-1 Gag protein.[27−30] In a notable example, we probed the dynamics of HIV-1 virus capsid assemblies and their interactions with the host factor cyclophilin A (CypA)[13] by MAS NMR at temperatures close to physiological, where dynamically averaged experimental parameters were interpreted in light of those calculated from MD trajectories.[8,13]

Here, we explore an alternative approach based on dynamic nuclear polarization (DNP)-enhanced MAS NMR spectroscopy at cryogenic temperatures and high magnetic fields to probe the conformational properties of large viral assemblies at atomic resolution and with high sensitivity. We examine two viral capsids: the human immunodeficiency 1 virus (HIV-1) capsid and the bacteriophage AP205 virus-like particles (VLPs). Viral capsids are unique compared to other classes of biomolecules, previously studied by DNP, such as amyloids or microcrystalline proteins studied by others previously,[31,32] because they are generally multicomponent assemblies that possess high curvature and often high symmetry and exhibit varying degrees of order and conformational flexibility.

In an earlier pioneering study, Havlin and Tycko showed that ensembles of unfolded and partially folded proteins could be trapped in glassy frozen solutions and realized that 2D solid-state NMR line shapes inform on conformational distributions.[33] This approach suggested that MAS NMR spectra of frozen solutions might provide immediate access to the signatures of each individual conformer and could be exploited in the context of dynamics studies to translate the dynamically averaged NMR parameters at room temperature into distributions of values.

Havlin and Tycko's study was conducted at 9.4 T, a field where cross-peak line shapes can be analyzed in terms of large conformational changes, as those induced by rapid chemical denaturation.[33] However, conformational averaging in folded assemblies leads to subtler chemical shift distributions, which are masked by homogeneous broadening, invariably accompanying MAS NMR spectra of biomolecules at cryogenic temperatures.[34] Here, we show that this problem can be addressed by studying samples with DNP at high magnetic fields, leveraging a new generation of instruments operating at 14.1 T and above. On the one hand, DNP drastically enhances the NMR signal, allowing the acquisition of 2D correlations in a matter of hours to days on a few milligrams of a sample.[35,36] On the other hand, the combination of cryogenic temperatures and high magnetic fields yields 2D line shapes that are dominated by inhomogeneous contributions,[37−40] facilitating their analysis in terms of rapid fluctuations within a conformational distribution using MD simulations.[41] This approach is well suited to probe the degree of dynamical disorder in these viral assemblies, and the associated motions can be quantified through an integrated DNP MAS NMR/MD simulation approach.

The level of detail elucidated in this study was inaccessible only a few years ago but is now possible using high-field DNP and state-of-the-art MD simulations. We envision that the integrated approach described here will be particularly useful for characterizing minor species and mobile sites in viral assemblies as well as in other biological systems of comparable complexity.

MATERIALS AND METHODS

Sample Preparation. Expression and purification of U-^{13}C, ^{15}N CA (HXB2 strain) were performed as reported previously.[9,42] Tubular assemblies of CA were prepared from 32 mg/mL protein solutions in 25 mM phosphate buffer (pH 5.5) containing 2.4 M NaCl. The solutions were incubated at 37 °C for 1 h and stored at 4 °C for subsequent experiments. The samples for DNP enhanced measurements of CA tubular assemblies containing 8 mM AMUPol (15-{[(7-oxyl-3,11-dioxa-7-azadispiro[5.1.5.3]hexadec-15-yl)carbamoyl][2-(2,5,8,11-tetraoxatridecan-13-ylamino)}-[3,11-dioxa-7-azadispiro[5.1.5.3]hexadec-7-yl])oxidanyl)[43] were prepared as reported previously.[44] A U-^{13}C, ^{15}N-labeled microcrystalline AP205 nucleocapsid was prepared as described previously.[45] For DNP measurements, the crystals were soaked in 10 mM AMUPol solution in the crystallization mother liquor (0.1 M HEPES at pH 7.5, 0.1 M NaCl, and 16% (w/v) deuterated PEG 4600) and then centrifuged in a 1.3 mm NMR rotor.

Transmission Electron Microscopy. The sample morphologies were characterized by TEM analysis, performed with a Zeiss CEM 902 transmission electron microscope operating at 80 kV. Samples were stained with ammonium molybdate (5%, w/v), deposited onto 400-mesh formvar/carbon-coated copper grids, and dried for 40 min. Some of the assemblies were analyzed using a Zeiss Libra 120 transmission electron microscope operating at 120 kV. Samples were stained with uranyl acetate (5%, w/v), deposited onto 400-mesh formvar/carbon-coated copper grids, and dried for 40 min in air. The copper grids were pretreated with a Pelco easiGlow Discharge Unit to deposit a charge so that the assemblies were uniformly spread on the grid surface and adhered to it.

MAS NMR Spectroscopy. MAS NMR spectra (19.96 T) of tubular assemblies of CA were acquired on a Bruker AVIII spectrometer equipped with a 3.2 mm E^{free} CPMAS HCN probe. The Larmor frequencies were 850.400 MHz (^{1}H) and 213.855 MHz (^{13}C). The spectra were collected at the MAS frequency of 14 kHz, and the temperature was maintained at 277 K. The typical pulse lengths were 2.9 μs for ^{1}H and 4.2 μs for ^{13}C. ^{1}H−^{13}C cross-polarization (CP) was performed with a linear amplitude ramp (80−100%); the CP contact time was 2 ms. The ^{13}C−^{13}C correlation spectrum was acquired using a Combined R2$_n^v$-driven (CORD)[46] experiment with a mixing time of 50 ms.

DOI: 10.1021/acs.jpcb.9b02293
J. Phys. Chem. B 2019, 123, 5048−5058

DNP-enhanced MAS NMR spectra of CA tubular assemblies were acquired in the Bruker Billerica laboratories on an Avance III SSNMR spectrometer equipped with a 3.2 mm triple-resonance low-temperature MAS probe. At 14.1 T, the Larmor frequencies were 600.080 MHz (^{1}H), 150.905 MHz (^{13}C), and 60.813 MHz (^{15}N). The microwave (MW) frequency was 395.18 GHz, and the MW irradiation generated by a second-harmonic gyrotron delivered 12 W of power to the sample. The measurements were performed at 109 K, and the sample temperature was calibrated using KBr.[47] The typical pulse lengths were 2.5 μs (^{1}H) and 4 μs (^{13}C), and the ^{1}H−^{13}C contact time was 2 ms. All spectra were acquired at the MAS frequency of 12.5 kHz, controlled by a Bruker MAS controller. For 2D and 3D NCACX correlation experiments, band selective magnetization transfer from ^{15}N to $^{13}C\alpha$ was performed using a spectrally induced filtering in combination with cross-polarization (SPECIFIC-CP)[48] contact time of 6.5 ms followed by a dipolar-assisted rotational resonance (DARR)[49,50] mixing time of 40 ms. For DNP-enhanced MAS NMR measurements at 18.8 T, the Larmor frequencies were 799.723 MHz (^{1}H) and 201.107 MHz (^{13}C), and the microwave frequency was 527 GHz. Data were recorded at a temperature of 110 K. The sample temperature was calibrated using KBr. The typical pulse lengths were 2.5 μs (^{1}H) and 4.75 μs (^{13}C), and the ^{1}H−^{13}C CP contact time was 2 ms. The MAS frequency was 10 kHz, and the proton-driven spin diffusion (PDSD)[51] mixing time was 60 ms.

The DNP-assisted measurements on AP205 nucleocapsids were performed on a Bruker spectrometer equipped with a 1.3 mm triple-resonance low-temperature DNP probe at 18.8 T (Larmor frequencies: ^{13}C = 201.107 MHz; ^{1}H = 799.720 MHz). The CORD mixing time was 100 ms, the MAS frequency was 40 kHz, and the temperature was 115 K.

Processing and Analysis of MAS NMR Spectra. The 2D NCACX and ^{13}C−^{13}C correlation spectra were processed in TopSpin using Gaussian and sine-bell squared apodization applied to the direct and indirect dimensions, respectively. The 3D NCACX spectrum was processed in NMRPipe[52] using 60° shifted sine-bell apodization, followed by a Lorentzian-to-Gaussian transformation in all dimensions. All data sets were analyzed in Sparky.[53]

Molecular Dynamics Simulations and Chemical Shift Predictions. MD simulations for 100 ns were performed on a CA monomer (HXB2 strain), as reported previously.[13] MD simulations of AP205 were performed on the dimeric subunit of the assembled capsid structure.[54] Bulk water and sodium/chloride ions were added using Visual Molecular Dynamics (VMD)[55] by setting the total concentration of NaCl to 0.15 M. The system was then equilibrated using ACEMD[56] for 2.1 ns at 300 K, and the simulation was run for 100 ns. The chemical shifts for individual substructures of the trajectory were predicted using SHIFTX.[57]

RESULTS AND DISCUSSION

DNP MAS NMR Spectra of HIV-1 Capsids and AP205 VLPs: Disorder versus Order. Mature HIV-1 capsids are cone-shaped assemblies of ∼1500 copies of the 231-residue capsid (CA) protein (Figure S1a, Supporting Information), a proteolytic cleavage product of the Gag polyprotein. HIV-1 capsids hold the viral genome and the proteins necessary for viral replication.[58,59] The capsid cones are assembled from ∼216 hexameric and 12 pentameric units of CA.[60−63] CA tubes, which have been studied extensively by cryo-EM[60,64] and MAS NMR spectroscopy,[3,4,8−10,13] capture the predominant symmetry element of the cones: a hexagonal lattice with a sixfold symmetry, assembled from CA monomers (Figure S1b, Supporting Information). In both conical and tubular assemblies, the N-terminal domains (NTDs) of CA (residues 1−149) form the outer surface of the tubular assemblies, while the inner surface is lined by C-terminal domains (CTDs) (residues 150−231).

For HIV CA, it has been established by us and others that the conformational plasticity of CA, directly linked to its internal dynamics, is critical for capsid assembly,[8,10,29,61,65−68] virus maturation,[9] and interactions with cellular host factors, such as CypA[13] and TRIM5α.[69] Atomic-level insights into the dynamics of CA assemblies and their complexes with CypA and TRIM5α CC-SPRY domains were obtained by monitoring molecular motions on nano- to millisecond timescales using MAS NMR in combination with MD simulations.[8,9,13,69] These studies revealed that the functionally important CypA loop region is highly flexible.[8,10,13] These dynamics were found to be a determining factor in HIV-1's escape from CypA dependence. We also recently reported that broad signals from dynamically disordered regions of HIV-1 capsid protein assemblies,[44,70] which are invisible at ambient temperatures, can be observed in frozen samples.[9,13]

AP205 bacteriophages are small RNA viruses with an icosahedral capsid shell that is made up of 178 copies of the coat protein[45,71] and a single copy of the maturation protein. In the absence of the maturation protein, 90 dimers of the AP205 coat protein assemble into stable VLPs. Recently, a complete model of the AP205 VLP has been derived from a crystal structure of an unassembled coat protein dimer together with solid-state NMR and cryo-electron microscopy (cryo-EM) data (Figure 1e). This model revealed a circular permutation of the coat protein, which allows both of its termini to be surface-exposed in assembled VLPs, tolerating insertions at the N- or C-termini.[54] Despite the high level of characterization already available, the mechanism of assembly and genome encapsidation is not completely understood, and there is currently no information about the level of local

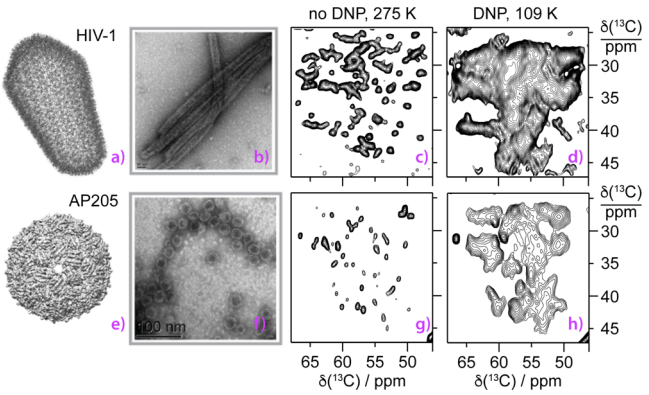

Figure 1. HIV-1 (top) and bacteriophage AP205 (bottom) viruses investigated by DNP-enhanced MAS NMR spectroscopy. (a) All-atom model of a mature HIV-1 capsid (PDB ID: 3J3Y).[61] (e) Cryo-EM reconstruction of AP205.[54] (b, f) Transmission electron microscopy (TEM) images. (c, d) Expansions of ^{13}C−^{13}C correlation spectra of CA tubular assemblies. (g, h) AP205 VLPs. Conditions were (c) 19.96 T, 277 K; (d) 14.1 T, 110 K, DNP-enhanced; (g) 23.4 T, 275 k; and (h) 18.8 T, 109 K, DNP-enhanced. For detailed experimental conditions, see Materials and Methods.

DOI: 10.1021/acs.jpcb.9b02293
J. Phys. Chem. B 2019, 123, 5048−5058

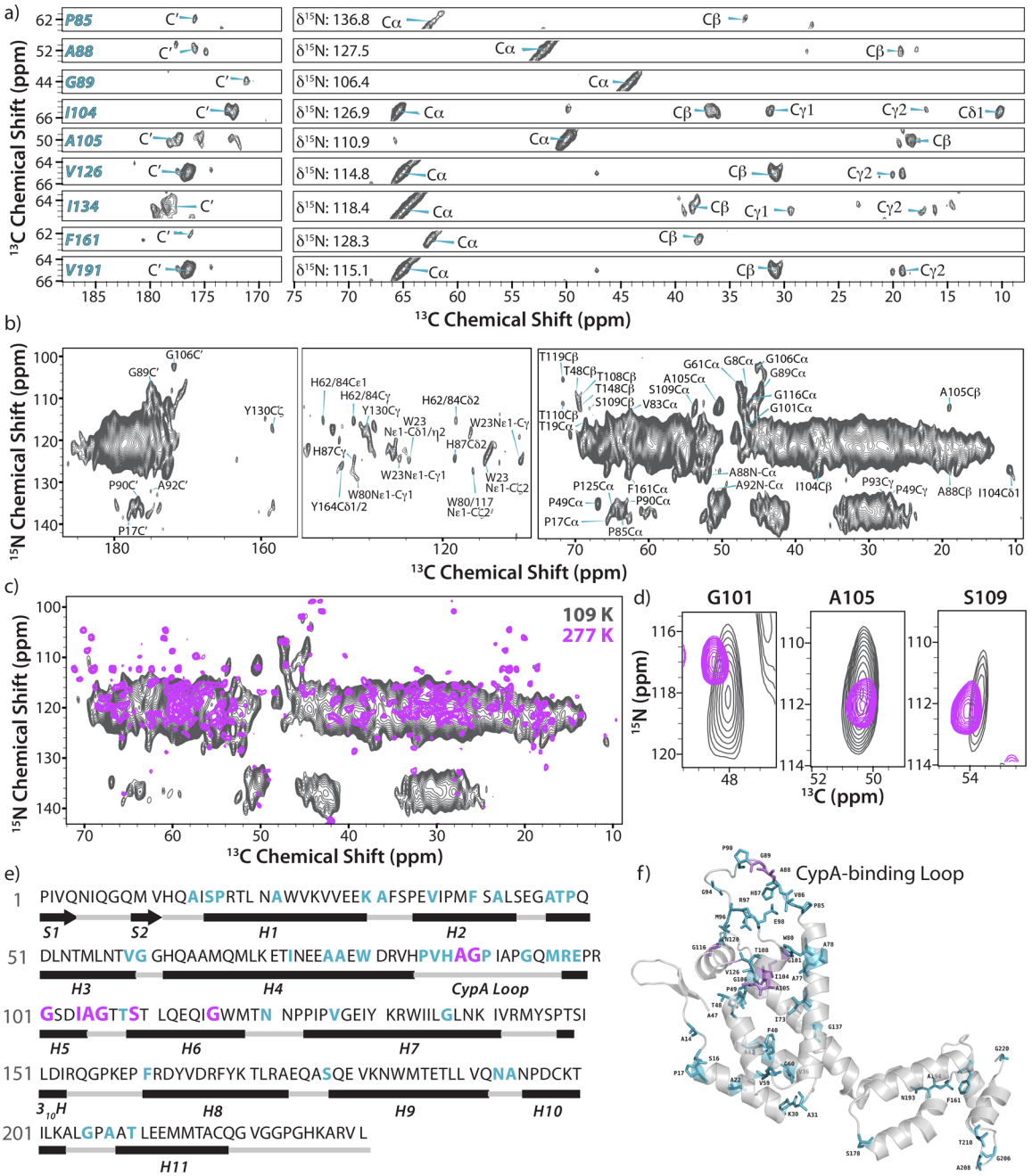

Figure 2. DNP-enhanced 2D and 3D NCACX correlation spectra of U-^{13}C, ^{15}N HIV-1 CA tubular assemblies acquired at 14.1 T and 109 K. (a) Selected 2D strips of the 3D NCACX spectrum showing well-resolved resonances and their assignments. (b) 2D NCACX spectrum. The MAS frequency was 12.5 KHz, the SPECIFIC-CP time for the NCA transfer was 6.5 ms, and the DARR mixing time was 40 ms. (c) Overlay of 2D NCACX spectra acquired under cryogenic temperatures with DNP (14.1 T, gray) and under ambient temperature conditions without DNP (21.1 T, magenta). (d) Expansion of (c) showing three representative, well-resolved resonances. (e) Primary amino acid sequence of CA with the secondary structure shown. (f) Position of amino acid residues observed and assigned by DNP-enhanced MAS NMR spectroscopy shown in the crystal structure of unassembled full-length CA (PDB: 3NTE). (e, f) Assigned residues are colored cyan, and residues for which chemical shift distributions were analyzed are colored magenta.

dynamics that can be accommodated within icosahedral viral capsid assemblies. An atomic-level characterization of the structure and dynamics of viral particles is essential for understanding virus assembly, virus evolution, virus−host interactions, and RNA genome recognition.

A comparison of ^{13}C−^{13}C correlation spectra of the two capsid assemblies acquired at ambient temperature (800 and 850 MHz) and under DNP conditions at 600 MHz (for HIV-1 CA) and 800 MHz (for AP205) fields is shown in Figure 1c,d,g,h. The ^{13}C resolution of the DNP-enhanced spectra acquired at around 109 K, lower than that of the ambient-temperature non-DNP data, is of the order of 1−1.8 ppm (as estimated from the resolved peaks in the NCACX spectrum shown in Figure 2b), which is considerably narrower than the DNP spectra of many proteins reported in the literature.[72] Line broadening in DNP spectra can be caused by homogeneous and inhomogeneous contributions. The effects of homogeneous contributions to the line widths can be

DOI: 10.1021/acs.jpcb.9b02293
J. Phys. Chem. B 2019, 123, 5048−5058

alleviated by increasing the strength of the static magnetic field, while the inhomogeneous contributions remain unaffected. As is evident in Figure 1d,h, there are a number of resolved peaks corresponding to individual amino acids. Interestingly, the line widths show variations from site to site. We hypothesized that the broader lines may be associated with the presence of motions and multiple conformers. We decided to explore this possibility further.

Heteronuclear DNP-Enhanced MAS NMR Spectra for HIV-1 CA Assemblies. The possible implications of dynamics observable in the DNP-enhanced MAS NMR spectra were first analyzed for HIV-1 CA assemblies. DNP-enhanced 2D MAS NMR spectra of tubular assemblies of HIV-1 CA and the Gag maturation intermediate containing CA and the 14-residue spacer peptide 1 (SP1), CA-SP1, were evaluated, and 64- or 20-fold sensitivity enhancements at 109 K were obtained for CA and CA-SP1, respectively. This enabled time-efficient acquisition of 2D homonuclear data sets and permitted detection of resonances for the flexible SP1 peptide region and determination of its secondary structure.[44] The resolution of these DNP-enhanced 2D homonuclear spectra was such that we could assign several side-chain and backbone resonances.[44] However, these data sets alone were insufficient for complete site-specific resonance assignments.

Therefore, 2D and 3D DNP-enhanced heteronuclear NCACX correlation spectra were recorded, which exhibit a remarkably high resolution (Figure 2). Furthermore, the acquisition times were only 0.6 and 17 h for the 2D and 3D spectra, respectively. Based on the 3D NCACX data set (Figure 2a) and available chemical shifts from solution and MAS NMR studies,[4,73] backbone and side-chain resonances for 44 residues were obtained. The 2D NCACX spectrum of tubular CA assemblies acquired at 109 K (14.1 T) is displayed in Figure 2b. Several well-resolved isolated resonances, particularly associated with the dynamic CypA-binding loop, were detected, similar to the 3D data set. In addition, resonances from several aromatic side-chain atoms are seen in the spectra and were readily assigned. Resonances of aromatic side chains generally exhibit low intensities in the ambient-temperature spectra, and their facile detection through DNP-based measurements is highly advantageous.

Spectral intensity is present for many amino acid residues of CA, as illustrated by the superposition of the NCACX spectra acquired under DNP and non-DNP conditions (Figure 2c). Interestingly, resonances for several proline residues, which were not observed at ambient temperature, exhibited high intensities, and the chemical shifts indicate that both cis- and trans-conformers are present (Figure S2, Supporting Information). The fact that we observed spectral intensity for most of the amino acids in both NTD and CTD suggests that either the DNP biradical diffused into the tubes or efficient spin diffusion from the exterior tube surface, lined by NTDs, to the interior lining of the tube comprising CTDs is present.

Overall, assignments were obtained for about 20% of the total number of amino acids in the CA sequence (Figure 2e). Residues with assigned resonances are highlighted on the structure of a single CA chain (Figure 2f). Resonances for 10 residues in the CypA loop, which is located on the surface of the assemblies (Figure S1, Supporting Information), were assigned. The CypA loop residues are highly mobile at ambient temperatures, and we have characterized their dynamics extensively.[13] Therefore, the presence of the corresponding resonances in the DNP-enhanced spectra allows us to benchmark the approach for conformational space sampling using cryogenic-temperature DNP data.

The temperature dependencies of the chemical shifts could be estimated from the DNP-enhanced spectra. Notably, chemical shift differences compared to ambient-temperature spectra are observed (Figure S3, Supporting Information) with larger than average differences (>1 ppm) occurring for resonances associated with mobile loops, compared to rigid regions. These large differences correlate with the reduced $^{1}H-^{15}N$ dipolar order parameters (Figures S4 and S5, Supporting Information), previously calculated on the basis of MD trajectories.[13] Given that $^{1}H-^{15}N$ dipolar order parameters are sensitive to motions on nano- to microsecond timescales, it appears that such motions can be indirectly inferred by examining the chemical shift differences at cryogenic conditions. This possibility is further explored below.

Residue-Specific Conformational Space Mapping by Combining DNP MAS NMR and MD Simulations. The possibility of exploiting spectral broadening introduced by conformational heterogeneity in DNP-enhanced spectra as a possible probe of dynamics was first explored for CA assemblies. The resolution of the DNP MAS NMR spectra of CA tubular assemblies is relatively high, compared to DNP spectra for the majority of other biological systems to date.[44] Nevertheless, as mentioned previously, with typical carbon-13 peak widths of 1.0 up to 1.8 ppm, the resolution is still considerably lower than in the ambient-temperature spectra.[13,44] Two factors have been shown previously to contribute to signal broadening and attenuation of intensities in DNP-enhanced measurements: conformational heterogeneity[34,41,74,75] and paramagnetic relaxation enhancements (PREs) due to the presence of a biradical.[39,41,76] The latter has been observed at ambient temperature for solvent-exposed regions of K^{+} channels integrated into membranes.[41] In our current study on tubular CA assemblies, relatively small increases in line widths were detected in $^{13}C-^{13}C$ homonuclear experiments at ambient temperatures;[44] therefore, although the DNP spectra are recorded at a different temperature, PREs are not expected to be a significant source of signal broadening in the current DNP studies.

Conformational heterogeneity is characterized by the presence of distinct conformers that are in dynamic exchange at ambient temperatures but are individually observable at cryogenic temperatures due to reduced molecular motions. As a result, line broadening in DNP-assisted spectra is expected to be residue-specific and difficult to predict without prior knowledge of the implicated motions. In general, the set of conformers that can contribute to each observable signal depends on multiple factors, such as the conformational space sampled by the individual residues, the interaction of side chains with solvent molecules in the frozen matrix, and the individual rates of the associated exchange/motional processes. Solvent molecules in the frozen glassy state will interact with amino acid side chains differently than in ambient-temperature solution. In a typical DNP experiment, the sample is slowly frozen to the desired cryogenic temperature with cooling rates as low as 1°/min[34] or as high as 10°/s.[74] An earlier study by Tycko and co-workers reported that, while these slow-freezing conditions trap equilibrium conformations, if a system is frozen quickly (e.g., freeze quenching by spraying a solution of a protein under investigation into cold isopentane), non-equilibrium states are additionally trapped, and mixtures of unfolded and fully folded molecules are found to be present.[77]

DOI: 10.1021/acs.jpcb.9b02293
J. Phys. Chem. B 2019, 123, 5048−5058

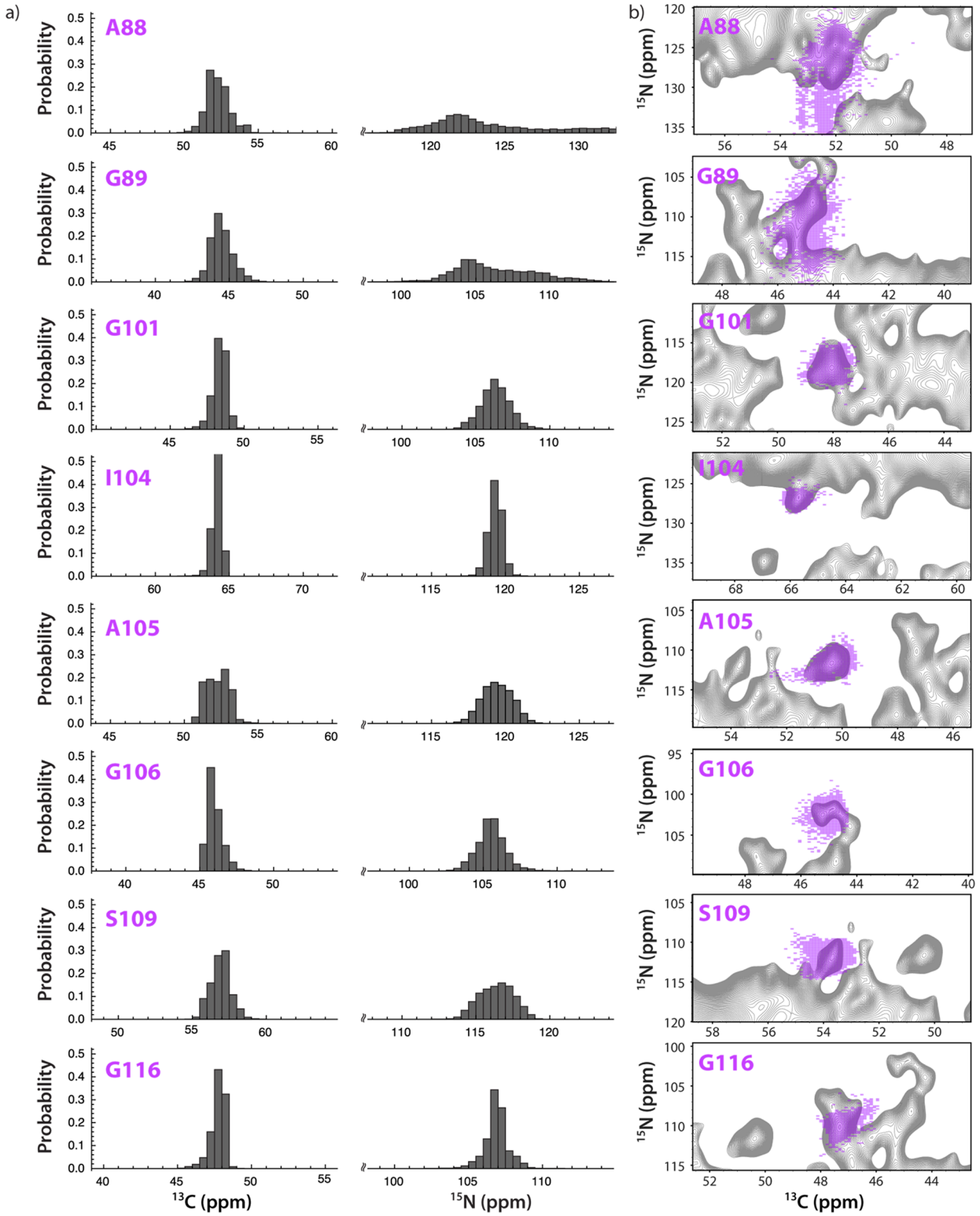

Figure 3. (a) Probability distributions of $^{13}C^{\alpha}$ and $^{15}N^{H}$ chemical shifts, calculated from 5000 substructures of the 100 ns MD trajectory for representative amino acids of HIV-1 CA. The range was set to ±8 ppm of the isotropic chemical shift to demonstrate the relative spread in chemical shift values. The isotropic chemical shifts were calculated using SHIFTX.[57] (b) Overlay of experimental contour plots (light pink) for well-resolved signals in the DNP-enhanced $^{15}N-^{13}C$ 2D NCACX correlation spectrum and chemical shift distribution maps for the corresponding residues (gray) of U-^{13}C, ^{15}N HIV-1 CA tubular assembly, calculated from 5000 substructures of 100 ns MD trajectories. Experimental conditions are the same as in Figure 2.

Therefore, the subset of conformers present in the DNP NMR experiments here is anticipated to reflect the equilibrium distribution of conformers.

MD simulations could potentially provide valuable information about the accessible conformational space and, within the practically reachable simulation timescales, should inform on

DOI: 10.1021/acs.jpcb.9b02293
J. Phys. Chem. B 2019, 123, 5048−5058

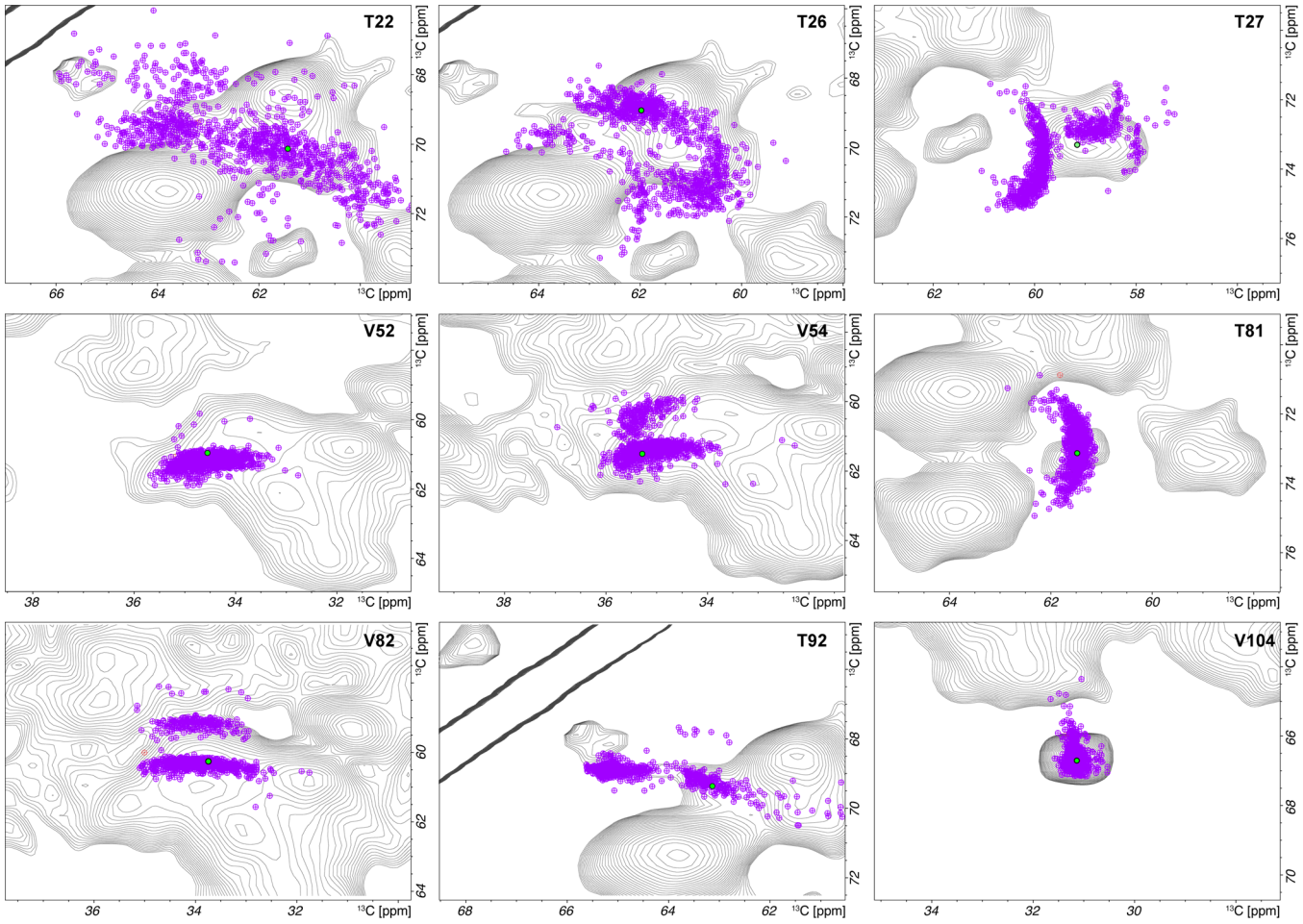

Figure 4. Overlay of two-dimensional chemical shift maps calculated from MD trajectories and ^{13}C−^{13}C correlations in a DNP-enhanced MAS NMR CORD spectrum of AP205 VLPs.

the equilibrium conformations trapped under the slow-freezing conditions employed in this work. Indeed, the chemical shift distributions derived on the basis of the MD trajectory show good agreement with experimental DNP MAS NMR results. The Baldus' group has previously used MD trajectories to estimate 1D ^{13}C line shapes from DNP-based experiments.[41] Here, we calculated chemical shifts from individual frames of the MD trajectories to obtain the distribution of conformers compatible with the observed shifts in 2D DNP MAS NMR experiments. To this end, 5000 frames were extracted from a 100 ns MD trajectory for CA tubular assemblies.

The effect of conformational heterogeneity in 2D heteronuclear DNP spectra of CA tubular assemblies is examined in Figure 3a, which depicts $^{13}C^{\alpha}$ and $^{15}N^{H}$ chemical shift distributions for the sets of conformers observed for eight representative residues, whose cross peaks are sufficiently resolved for the analysis, extracted from the MD conformer ensemble. The distribution of chemical shift values over the course of the MD trajectory is displayed in Figure 3a. Not surprisingly, residues that reside in the flexible CypA loop (e.g., A88 and G89) exhibit broader chemical shift distributions than those in more rigid regions, such as G116. This is qualitatively borne out by our data: the degree of molecular motion (as determined by the extent of the attenuation of dipolar order parameters with respect to the rigid limit values) correlates with the chemical shift distribution width (see Figure S4 of the Supporting Information). Dynamic residues, such as A88 and G89, exhibit broader chemical shift distributions compared to rigid residues, such as A105, S109, and G116.

Furthermore, the variability in $^{15}N^{H}$ chemical shifts is larger than that in $^{13}C^{\alpha}$ shifts, both based on the MD simulations (Figure 3a) as well as the experiment (Figure 2d), suggesting that conformational heterogeneity will result in more extensive broadening in the ^{15}N dimension than in the ^{13}C dimension. In contrast, the line widths (in parts per million) in the non-DNP spectra acquired at ambient conditions are very similar in the ^{15}N and ^{13}C dimensions. Therefore, the overall nonuniform increase in signal widths under DNP conditions is a strong indication that the predominant underlying cause for broadening is conformational heterogeneity, directly related to the relative flexibility of individual residues. Consequently, without the knowledge of the conformational space that is sampled by an individual residue, the extent of spectral broadening is difficult to predict. However, it becomes accessible through MD simulations.

To test the above assertion further, experimental 2D DNP line shapes were compared with those simulated on the basis of the individual conformers in the MD trajectory for several representative residues. The simulated chemical shift distributions for every pair of $^{13}C^{\alpha}$ and $^{15}N^{H}$ chemical shifts based on 5000 snapshots of a 100 ns MD trajectory are weighted with respect to abundance: the higher the frequency of a particular chemical shift pair, the brighter the spot (Figure 3b). The agreement between the simulated and experimental contour

DOI: 10.1021/acs.jpcb.9b02293
J. Phys. Chem. B 2019, 123, 5048−5058

maps is generally very good and is applicable to both rigid residues (G101, I104, A105, G106, S109, and G116) and the dynamic residue G89. A superposition of the chemical shift distribution map generated for all amino acids and the experimental DNP-enhanced NCACX spectrum is provided in Figure S6 (Supporting Information). The agreement of the experimental shifts with the MD-derived chemical shift maps suggests that the conformers captured by MD are representative of the accessible conformational space despite the fact that the sample freezing rates were slow in the current study. Indirectly, this assertion is supported by the fact that the use of shorter MD trajectories (up to 10 ns) does not reproduce the breadth of the observed chemical shift distributions for dynamic residues, as illustrated in Figure S7 (Supporting Information).

Not for all residues is a quantitative agreement observed. For example, for the dynamic A88 residue, the experimental and calculated shifts are different. This discrepancy cannot be explained by a PRE effect since no line broadening is observed, and the experimental peaks are narrower than the calculated distributions. One possibility may be that not all conformers can be frozen out during the slow cooling, although this hypothesis remains to be tested. Interestingly, the experimental $^{1}H-^{15}N$ dipolar order parameters for A88 at 4 °C also indicated that this residue is less dynamic than predicted by MD simulations (S^{exp} = 0.39 vs S^{MD} = 0.11 for the $^{1}H-^{15}N$ bond).[13] Furthermore, PRE-induced spectral broadening is expected to be relatively homogeneous, which is not borne out in the comparison of the simulated and experimental line shapes (Figure 3), and the presence or absence of the PRE effect may depend on the morphology of the sample, nature, and concentration of the biradical.[41,76,78]

The different extents to which $^{13}C^{\alpha}$ and $^{15}N^{H}$ chemical shifts are affected by dynamics, as observed experimentally and through MD simulations, demonstrate that both of these nuclei should be taken into consideration when analyzing the conformational space from experiments conducted at cryogenic temperatures, where molecular motions are restricted. Such an analysis will potentially allow for estimating the entire conformational space and dynamics in the HIV-1 protein and other viral assemblies and will be pursued in conjunction with detailed studies aimed at estimating the relative contributions of PRE-induced or conformational heterogeneity-associated spectral broadening in the future.

Intact Viral Assemblies: Bacteriophage AP205. Intrigued by the findings on the HIV-1 CA assemblies, we examined the ^{13}C chemical shift distributions in the VLPs of the bacteriophage AP205 coat protein on the basis of 1000 frames extracted from a 100 ns MD trajectory. Resonance assignments derived from the 2D DNP-enhanced spectra were validated by the comparison with the assignments reported by us previously on the basis of the 2D and 3D spectra acquired at 275 K,[54] with minor temperature-induced chemical shift changes. A superposition of the experimental 2D $^{13}C-^{13}C$ correlation spectra with simulated chemical shift distribution maps is provided in Figure 4. Qualitatively, the simulated chemical shift distributions for AP205 exhibit reasonable agreement with the experimental spectra, suggesting that conformers in the MD trajectories, which would be averaged at ambient temperatures, are trapped and become detectable at cryogenic temperatures in the DNP experiments. It is worth noting that, for AP205, the analysis was performed for $C^{\alpha}-C^{\beta}$ correlations, while for the HIV-1 CA, it was performed for the $N^{H}-C^{\alpha}$ correlations between the backbone atoms. This may explain why the agreement is slightly less convincing than for the line shapes presented in Figure 3

The approach presented here is in its early stages of development and has inherent limitations, such as (i) the lack of clear procedure at the current time to assure that the states trapped at cryogenic temperatures represent all of the equilibrium conformers and (ii) MD simulations sampling the entire equilibrium conformational space. To gain systematic understanding into these issues and to overcome these, further investigation spanning multiple systems and multiple conditions is needed.

CONCLUSIONS

We applied an integrated DNP MAS NMR/MD approach for analyzing the structure and dynamics in HIV-1 capsid assemblies and bacteriophage AP205 VLPs. The study was enabled by DNP-enhanced MAS NMR spectroscopy that yielded considerable sensitivity gains. It was then possible to record 2D and 3D heteronuclear correlation spectra in a fraction of time, compared to the acquisition of conventional data sets. We show that, at low temperatures, individual conformers, which are in dynamic exchange at ambient temperatures, are frozen out such that they exhibit separate lines in ^{13}C and ^{15}N NMR spectra. The detected distinct $^{13}C/^{15}N$ chemical shift distributions are in accordance with the extent of dynamics and the accessible conformational space in HIV-1 CA and AP205 assemblies displayed by the chemical shift distributions, calculated from MD trajectories. A remarkable qualitative agreement between the ^{15}N and ^{13}C 2D line shapes and calculated chemical shift distributions is observed. Our results suggest that DNP-based experiments combined with MD simulations can be used to probe both the structure and conformational dynamics. Furthermore, the integrated methodology described here is a powerful means to study functionally relevant dynamics in complex biological systems, including but not limited to viruses.

ASSOCIATED CONTENT

Supporting Information

The Supporting Information is available free of charge on the ACS Publications website at DOI: 10.1021/acs.jpcb.9b02293.

^{13}C and ^{15}N chemical shifts for resonances assigned with DNP-enhanced spectra, a plot showing differences in the chemical shifts for DNP and ambient-temperature measurements, and an overlay of simulated chemical shift distribution maps for all amino acid residues and the experimental DNP NCACX spectrum (PDF)

AUTHOR INFORMATION

Corresponding Authors

*E-mail: guido.pintacuda@ens-lyon.fr (G.P.).
*E-mail: Anne.Lesage@ens-lyon.fr (A.L.).
*E-mail: amg100@pitt.edu (A.M.G.).
*E-mail: tpolenov@udel.edu (T.P.).

ORCID

Rupal Gupta: 0000-0001-8637-6129
Manman Lu: 0000-0002-4156-4975
Guangjin Hou: 0000-0001-8216-863X
Jochem Struppe: 0000-0001-9001-5991
Kristaps Jaudzems: 0000-0003-3922-2447

DOI: 10.1021/acs.jpcb.9b02293
J. Phys. Chem. B 2019, 123, 5048−5058

Lyndon Emsley: 0000-0003-1360-2572
Guido Pintacuda: 0000-0001-7757-2144
Anne Lesage: 0000-0003-1958-2840
Angela M. Gronenborn: 0000-0001-9072-3525
Tatyana Polenova: 0000-0002-0346-1131

Present Addresses

†M.C.: Amgen, Inc., 360 Binney Street, Cambridge, Massachusetts 02142, United States
#R.G.: Department of Chemistry, College of Staten Island, Building 6S, Room 214, 2800 Victory Boulevard, Staten Island, New York, New York 10314, United States
●G.H.: State Key Laboratory of Catalysis, Dalian Institute of Chemical Physics, Chinese Academy of Sciences, Dalian 116023, China

Notes

The authors declare no competing financial interest.

■ ACKNOWLEDGMENTS

This work was supported by the National Institutes of Health (NIH grant no. P50AI150481 to A.M.G. and T.P.) and is a contribution from the Pittsburgh Center for HIV Protein Interactions and was also supported by GRAL (ANR-10-LABX-49-01) and Finovi (Fondation Innovations en Infectiologie). We acknowledge the support of the NSF CHE0959496 grant for acquisition of the 850 MHz NMR spectrometer and of the NIGMS P30GM110758 grant for the support of core instrumentation infrastructure at the University of Delaware. We thank Christopher J. Langmead at the Carnegie Mellon University for providing MD trajectories of the CA monomer. The work used the platforms of the Grenoble Instruct-ERIC Centre (ISBG; UMS 3518 CNRS-CEA-UJA-EMBL) with the support from FRISBI (no. ANR-10-INSB-05-02) and GRAL (no. ANR-10-LABX-49-01) within the Grenoble Partnership for Structural Biology (PSB). The electron microscope facility is supported by the Rhône-Alpes Region, Fondation Recherche Medicale (FRM), Fonds FEDER, Centre National de la Recherche Scientifique (CNRS), CEA, University of Grenoble, EMBL, and GIS-Infrastructures en Biologie Sante et Agronomie (IBISA). We thank Fenel Daphna, Christine Moriscot, and Guy Schoehn from the Electron Microscopy platform of the Integrated Structural Biology of Grenoble (ISBG, UMS 3518). We thank the European Synchrotron Radiation Facility (ESRF).

■ REFERENCES

(1) Goldbourt, A.; Gross, B. J.; Day, L. A.; McDermott, A. E. Filamentous Phage Studied by Magic-Angle Spinning NMR: Resonance Assignment and Secondary Structure of the Coat Protein in Pf1. *J. Am. Chem. Soc.* **2007**, *129*, 2338−2344.
(2) Lorieau, J. L.; Day, L. A.; McDermott, A. E. Conformational Dynamics of an Intact Virus: Order Parameters for the Coat Protein of Pf1 Bacteriophage. *Proc. Natl. Acad. Sci. U. S. A.* **2008**, *105*, 10366−10371.
(3) Chen, B.; Tycko, R. Structural and Dynamical Characterization of Tubular HIV-1 Capsid Protein Assemblies by Solid State Nuclear Magnetic Resonance and Electron Microscopy. *Protein Sci.* **2010**, *19*, 716−730.
(4) Han, Y.; Ahn, J.; Concel, J.; Byeon, I. J. L.; Gronenborn, A. M.; Yang, J.; Polenova, T. Solid-State NMR Studies of HIV-1 Capsid Protein Assemblies. *J. Am. Chem. Soc.* **2010**, *132*, 1976−1987.
(5) Morag, O.; Abramov, G.; Goldbourt, A. Similarities and Differences within Members of the Ff Family of Filamentous Bacteriophage Viruses. *J. Phys. Chem. B* **2011**, *115*, 15370−15379.
(6) Abramov, G.; Morag, O.; Goldbourt, A. Magic-Angle Spinning NMR of a Class I Filamentous Bacteriophage Virus. *J. Phys. Chem. B* **2011**, *115*, 9671−9680.
(7) Sergeyev, I. V.; Day, L. A.; Goldbourt, A.; McDermott, A. E. Chemical Shifts for the Unusual DNA Structure in Pf1 Bacteriophage from Dynamic-Nuclear-Polarization-Enhanced Solid-State NMR Spectroscopy. *J. Am. Chem. Soc.* **2011**, *133*, 20208−20217.
(8) Byeon, I. J. L.; Hou, G.; Han, Y.; Suiter, C. L.; Ahn, J.; Jung, J.; Byeon, C. H.; Gronenborn, A. M.; Polenova, T. Motions on the Millisecond Time Scale and Multiple Conformations of HIV-1 Capsid Protein: Implications for Structural Polymorphism of CA Assemblies. *J. Am. Chem. Soc.* **2012**, *134*, 6455−6466.
(9) Han, Y.; Hou, G.; Suiter, C. L.; Ahn, J.; Byeon, I.-J. L.; Lipton, A. S.; Burton, S.; Hung, I.; Gor'kov, P. L.; Gan, Z. H.; et al. Magic Angle Spinning NMR Reveals Sequence-Dependent Structural Plasticity, Dynamics, and the Spacer Peptide 1 Conformation in HIV-1 Capsid Protein Assemblies. *J. Am. Chem. Soc.* **2013**, *135*, 17793−17803.
(10) Bayro, M. J.; Chen, B.; Yau, W. M.; Tycko, R. Site-Specific Structural Variations Accompanying Tubular Assembly of the HIV-1 Capsid Protein. *J. Mol. Biol.* **2014**, *426*, 1109−1127.
(11) Morag, O.; Abramov, G.; Goldbourt, A. Complete Chemical Shift Assignment of the ssDNA in the Filamentous Bacteriophage Fd Reports on its Conformation and on its Interface with the Capsid Shell. *J. Am. Chem. Soc.* **2014**, *136*, 2292−2301.
(12) Barbet-Massin, E.; Felletti, M.; Schneider, R.; Jehle, S.; Communie, G.; Martinez, N.; Jensen, M. R.; Ruigrok, R. W. H.; Emsley, L.; Lesage, A.; et al. Insights into the Structure and Dynamics of Measles Virus Nucleocapsids by ^{1}H-detected Solid-State NMR. *Biophys. J.* **2014**, *107*, 941−946.
(13) Lu, M.; Hou, G.; Zhang, H.; Suiter, C. L.; Ahn, J.; Byeon, I.-J. L.; Perilla, J. R.; Langmead, C. J.; Hung, I.; Gor'kov, P. L.; et al. Dynamic Allostery Governs Cyclophilin A-HIV Capsid Interplay. *Proc. Natl. Acad. Sci. U. S. A.* **2015**, *112*, 14617−14622.
(14) Palmer, A. G., III NMR Probes of Molecular Dynamics: Overview and Comparison with Other Techniques. *Annu. Rev. Biophys. Biomol. Struct.* **2001**, *30*, 129−55.
(15) Palmer, A. G. Enzyme Dynamics from NMR Spectroscopy. *Acc. Chem. Res.* **2015**, *48*, 457−65.
(16) Salmon, L.; Blackledge, M. Investigating Protein Conformational Energy Landscapes and Atomic Resolution Dynamics from NMR Dipolar Couplings: A Review. *Rep. Prog. Phys.* **2015**, *78*, 126601.
(17) Lisi, G. P.; Loria, J. P. Using NMR Spectroscopy to Elucidate the Role of Molecular Motions in Enzyme Function. *Prog. Nucl. Magn. Reson. Spectrosc.* **2016**, *92-93*, 1−17.
(18) Williams, J. C.; McDermott, A. E. Dynamics of the Flexible Loop of Triosephosphate Isomerase: The Loop Motion Is Not Ligand Gated. *Biochemistry* **1995**, *34*, 8309−19.
(19) Quinn, C. M.; McDermott, A. E. Quantifying Conformational Dynamics Using Solid-State $R_{1\rho}$ Experiments. *J. Magn. Reson.* **2012**, *222*, 1−7.
(20) Lewandowski, J. R.; Halse, M. E.; Blackledge, M.; Emsley, L. Direct Observation of Hierarchical Protein Dynamics. *Science* **2015**, *348*, 578−81.
(21) Tollinger, M.; Sivertsen, A. C.; Meier, B. H.; Ernst, M.; Schanda, P. Site-Resolved Measurement of Microsecond-to-Millisecond Conformational-Exchange Processes in Proteins by Solid-State NMR Spectroscopy. *J. Am. Chem. Soc.* **2012**, *134*, 14800−7.
(22) Krushelnitsky, A.; Gauto, D.; Rodriguez Camargo, D. C.; Schanda, P.; Saalwächter, K. Microsecond Motions Probed by Near-Rotary-Resonance $R_{1\rho}$ ^{15}N MAS NMR Experiments: The Model Case of Protein Overall-Rocking in Crystals. *J. Biomol. NMR* **2018**, *71*, 53−67.
(23) Zinkevich, T.; Chevelkov, V.; Reif, B.; Saalwächter, K.; Krushelnitsky, A. Internal Protein Dynamics on Ps to μs Timescales as Studied by Multi-Frequency ^{15}N Solid-State NMR Relaxation. *J. Biomol. NMR* **2013**, *57*, 219−35.

DOI: 10.1021/acs.jpcb.9b02293
J. Phys. Chem. B 2019, 123, 5048−5058

(24) Quinn, C. M.; Polenova, T. Structural Biology of Supramolecular Assemblies by Magic-Angle Spinning NMR Spectroscopy. *Q. Rev. Biophys.* **2017**, *50*, 1−44.
(25) Mateu, M. G. Assembly, Stability and Dynamics of Virus Capsids. *Arch. Biochem. Biophys.* **2013**, *531*, 65−79.
(26) Milles, S.; Jensen, M. R.; Lazert, C.; Guseva, S.; Ivashchenko, S.; Communie, G.; Maurin, D.; Gerlier, D.; Ruigrok, R. W. H.; Blackledge, M. An Ultraweak Interaction in the Intrinsically Disordered Replication Machinery Is Essential for Measles Virus Function. *Science Advances* **2018**, *4*, eaat7778.
(27) Jensen, M. R.; Bernadó, P.; Houben, K.; Blanchard, L.; Marion, D.; Ruigrok, R. W.; Blackledge, M. Structural Disorder within Sendai Virus Nucleoprotein and Phosphoprotein: Insight into the Structural Basis of Molecular Recognition. *Protein Pept. Lett.* **2010**, *17*, 952−60.
(28) Labaronne, A.; Milles, S.; Donchet, A.; Jensen, M. R.; Blackledge, M.; Bourhis, J.-M.; Ruigrok, R. W. H.; Crépin, T. Structural Analysis of the Complex between Influenza B Nucleoprotein and Human importin-α. *Sci. Rep.* **2017**, *7*, 17164.
(29) Deshmukh, L.; Ghirlando, R.; Clore, G. M. Conformation and Dynamics of the Gag Polyprotein of the Human Immunodeficiency Virus 1 Studied by NMR Spectroscopy. *Proc. Natl. Acad. Sci. U. S. A.* **2015**, *112*, 3374−9.
(30) Baronti, L.; Erales, J.; Habchi, J.; Felli, I. C.; Pierattelli, R.; Longhi, S. Dynamics of the Intrinsically Disordered C-Terminal Domain of the Nipah Virus Nucleoprotein and Interaction with the X Domain of the Phosphoprotein as Unveiled by NMR Spectroscopy. *ChemBioChem* **2015**, *16*, 268−76.
(31) Debelouchina, G. T.; Bayro, M. J.; Fitzpatrick, A. W.; Ladizhansky, V.; Colvin, M. T.; Caporini, M. A.; Jaroniec, C. P.; Bajaj, V. S.; Rosay, M.; Macphee, C. E.; et al. Higher Order Amyloid Fibril Structure by MAS NMR and DNP Spectroscopy. *J. Am. Chem. Soc.* **2013**, *135*, 19237−19247.
(32) Geiger, M.-A.; Orwick-Rydmark, M.; Märker, K.; Franks, W. T.; Akhmetzyanov, D.; Stöppler, D.; Zinke, M.; Specker, E.; Nazaré, M.; Diehl, A.; et al. Temperature Dependence of Cross-Effect Dynamic Nuclear Polarization in Rotating Solids: Advantages of Elevated Temperatures. *Phys. Chem. Chem. Phys.* **2016**, *18*, 30696−30704.
(33) Havlin, R. H.; Tycko, R. Probing Site-Specific Conformational distributions in Protein Folding with Solid-State NMR. *Proc. Natl. Acad. Sci. U. S. A.* **2005**, *102*, 3284−9.
(34) Linden, A. H.; Franks, W. T.; Akbey, U.; Lange, S.; van Rossum, B. J.; Oschkinat, H. Cryogenic Temperature Effects and Resolution upon Slow Cooling of Protein Preparations in Solid State NMR. *J. Biomol. NMR* **2011**, *51*, 283−92.
(35) Ni, Q. Z.; Daviso, E.; Can, T. V.; Markhasin, E.; Jawla, S. K.; Swager, T. M.; Temkin, R. J.; Herzfeld, J.; Griffin, R. G. High Frequency Dynamic Nuclear Polarization. *Acc. Chem. Res.* **2013**, *46*, 1933−1941.
(36) Akbey, Ü.; Oschkinat, H. Structural Biology Applications of solid state MAS DNP NMR. *J. Magn. Reson.* **2016**, *269*, 213−224.
(37) Sergeyev, I. V.; Itin, B.; Rogawski, R.; Day, L. A.; McDermott, A. E. Efficient Assignment and NMR Analysis of an Intact Virus Using Sequential Side-Chain Correlations and DNP Sensitization. *Proc. Natl. Acad. Sci. U. S. A.* **2017**, *114*, 5171−5176.
(38) Fricke, P.; Mance, D.; Chevelkov, V.; Giller, K.; Becker, S.; Baldus, M.; Lange, A. High Resolution Observed in 800 MHz DNP Spectra of Extremely Rigid Type III Secretion Needles. *J. Biomol. NMR* **2016**, *65*, 121−6.
(39) Jaudzems, K.; Bertarello, A.; Chaudhari, S. R.; Pica, A.; Cala-De Paepe, D.; Barbet-Massin, E.; Pell, A. J.; Akopjana, I.; Kotelovica, S.; Gajan, D.; et al. Dynamic Nuclear Polarization-Enhanced Biomolecular NMR Spectroscopy at High Magnetic Field with Fast Magic-Angle Spinning. *Angew. Chem., Int. Ed.* **2018**, *57*, 7458−7462.
(40) Uluca, B.; Viennet, T.; Petrovic, D.; Shaykhalishahi, H.; Weirich, F.; Gonulalan, A.; Strodel, B.; Etzkorn, M.; Hoyer, W.; Heise, H. DNP-Enhanced MAS NMR: A Tool to Snapshot Conformational Ensembles of α-Synuclein in Different States. *Biophys. J.* **2018**, *114*, 1614−1623.
(41) Koers, E. J.; van der Cruijsen, E. A. W.; Rosay, M.; Weingarth, M.; Prokofyev, A.; Sauvée, C.; Ouari, O.; van der Zwan, J.; Pongs, O.; Tordo, P.; et al. NMR-Based Structural Biology Enhanced by Dynamic Nuclear Polarization at High Magnetic Field. *J. Biomol. NMR* **2014**, *60*, 157−68.
(42) Sun, S.; Han, Y.; Paramasivam, S.; Yan, S.; Siglin, A. E.; Williams, J. C.; Byeon, I.-J. L.; Ahn, J.; Gronenborn, A. M.; Polenova, T. Solid-State NMR Spectroscopy of Protein Complexes. *Methods Mol. Biol.* **2012**, *831*, 303−331.
(43) Sauvée, C.; Rosay, M.; Casano, G.; Aussenac, F.; Weber, R. T.; Ouari, O.; Tordo, P. Highly Efficient, Water-Soluble Polarizing Agents for Dynamic Nuclear Polarization at High Frequency. *Angew. Chem., Int. Ed.* **2013**, *52*, 10858−10861.
(44) Gupta, R.; Lu, M.; Hou, G.; Caporini, M. A.; Rosay, M.; Maas, W.; Struppe, J.; Suiter, C.; Ahn, J.; Byeon, I. J.; et al. Dynamic Nuclear Polarization Enhanced MAS NMR Spectroscopy for Structural Analysis of HIV-1 Protein Assemblies. *J. Phys. Chem. B* **2016**, *120*, 329−39.
(45) Andreas, L. B.; Jaudzems, K.; Stanek, J.; Lalli, D.; Bertarello, A.; Le Marchand, T.; Cala-De Paepe, D.; Kotelovica, S.; Akopjana, I.; Knott, B.; et al. Structure of Fully Protonated Proteins by Proton-Detected Magic-Angle Spinning NMR. *Proc. Natl. Acad. Sci. U. S. A.* **2016**, *113*, 9187−9192.
(46) Hou, G.; Yan, S.; Trébosc, J.; Amoureux, J. P.; Polenova, T. Broadband Homonuclear Correlation Spectroscopy Driven by Combined $R2^{n}_{v}$ Sequences under Fast Magic Angle Spinning for NMR Structural Analysis of Organic and Biological Solids. *J. Magn. Reson.* **2013**, *232*, 18−30.
(47) Thurber, K. R.; Tycko, R. Measurement of Sample Temperatures under Magic-Angle Spinning from the Chemical Shift and Spin-Lattice Relaxation Rate of ^{79}Br in KBr Powder. *J. Magn. Reson.* **2009**, *196*, 84−87.
(48) Baldus, M.; Petkova, A. T.; Herzfeld, J.; Griffin, R. G. Cross Polarization in the Tilted Frame: Assignment and Spectral Simplification in Heteronuclear Spin Systems. *Mol. Phys.* **1998**, *95*, 1197−1207.
(49) Takegoshi, K.; Nakamura, S.; Terao, T. ^{13}C-^{1}H Dipolar-Assisted Rotational Resonance in Magic-Angle Spinning NMR. *Chem. Phys. Lett.* **2001**, *344*, 631−637.
(50) Takegoshi, K.; Nakamura, S.; Terao, T. ^{13}C-^{1}H Dipolar-Driven ^{13}C-^{13}C Recoupling without ^{13}C RF Irradiation in Nuclear Magnetic Resonance of Rotating Solids. *J. Chem. Phys.* **2003**, *118*, 2325−2341.
(51) Bloembergen, N. On the Interaction of Nuclear Spins in a Crystalline Lattice. *Physica* **1949**, *15*, 386−426.
(52) Delaglio, F.; Grzesiek, S.; Vuister, G. W.; Zhu, G.; Pfeifer, J.; Bax, A. NMRPipe - a Multidimensional Spectral Processing System Based on Unix Pipes. *J. Biomol. NMR* **1995**, *6*, 277−293.
(53) Goddard, T. D.; Kneller, D. G. *SPARKY*, version 3.114; University of California, San Francisco, 2008.
(54) Shishovs, M.; Rumnieks, J.; Diebolder, C.; Jaudzems, K.; Andreas, L. B.; Stanek, J.; Kazaks, A.; Kotelovica, S.; Akopjana, I.; Pintacuda, G.; et al. Structure of AP205 Coat Protein Reveals Circular Permutation in ssRNA Bacteriophages. *J. Mol. Biol.* **2016**, *428*, 4267−4279.
(55) Humphrey, W.; Dalke, A.; Schulten, K. VMD: Visual Molecular Dynamics. *J. Mol. Graphics* **1996**, *14*, 33−38.
(56) Harvey, M. J.; Giupponi, G.; Fabritiis, G. D. ACEMD: Accelerating Biomolecular Dynamics in the Microsecond Time Scale. *J. Chem. Theory. Comput.* **2009**, *5*, 1632−1639.
(57) Neal, S.; Nip, A. M.; Zhang, H.; Wishart, D. S. Rapid and Accurate Calculation of Protein ^{1}H, ^{13}C and ^{15}N Chemical Shifts. *J. Biomol. NMR* **2003**, *26*, 215−240.
(58) Engelman, A.; Cherepanov, P. The Structural Biology of HIV-1: Mechanistic and Therapeutic Insights. *Nat. Rev. Microbiol.* **2012**, *10*, 279−90.
(59) Freed, E. O. HIV-1 Assembly, Release and Maturation. *Nat. Rev. Microbiol.* **2015**, *13*, 484−96.

DOI: 10.1021/acs.jpcb.9b02293
J. Phys. Chem. B 2019, 123, 5048−5058

(60) Ganser-Pornillos, B. K.; Cheng, A.; Yeager, M. Structure of Full-Length HIV-1 CA: A Model for the Mature Capsid Lattice. *Cell* **2007**, *131*, 70−79.
(61) Zhao, G.; Perilla, J. R.; Yufenyuy, E. L.; Meng, X.; Chen, B.; Ning, J.; Ahn, J.; Gronenborn, A. M.; Schulten, K.; Aiken, C.; et al. Mature HIV-1 Capsid Structure by Cryo-Electron Microscopy and all-Atom Molecular Dynamics. *Nature* **2013**, *497*, 643−646.
(62) Ganser, B. K.; Li, S.; Klishko, V. Y.; Finch, J. T.; Sundquist, W. I. Assembly and Analysis of Conical Models for the HIV-1 Core. *Science* **1999**, *283*, 80−3.
(63) Li, S.; Hill, C. P.; Sundquist, W. I.; Finch, J. T. Image Reconstructions of Helical Assemblies of the HIV-1 CA Protein. *Nature* **2000**, *407*, 409−13.
(64) Byeon, I.-J. L.; Meng, X.; Jung, J.; Zhao, G.; Yang, R.; Ahn, J.; Shi, J.; Concel, J.; Aiken, C.; Zhang, P.; et al. Structural Convergence between Cryo-EM and NMR Reveals Intersubunit Interactions Critical for HIV-1 Capsid Function. *Cell* **2009**, *139*, 780−790.
(65) Chen, B.; Tycko, R. Simulated Self-Assembly of the HIV-1 Capsid: Protein Shape and Native Contacts Are Sufficient for Two-Dimensional Lattice Formation. *Biophys. J.* **2011**, *100*, 3035−3044.
(66) Deshmukh, L.; Schwieters, C. D.; Grishaev, A.; Ghirlando, R.; Baber, J. L.; Clore, G. M. Structure and Dynamics of Full-Length HIV-1 Capsid Protein in Solution. *J. Am. Chem. Soc.* **2013**, *135*, 16133−47.
(67) Müller, B.; Krijnse-Locker, J. Imaging of HIV Assembly and Release. *Methods Mol. Biol.* **2014**, *1087*, 167−184.
(68) Gres, A. T.; Kirby, K. A.; KewalRamani, V. N.; Tanner, J. J.; Pornillos, O.; Sarafianos, S. G. X-Ray Crystal Structures of Native HIV-1 Capsid Protein Reveal Conformational Variability. *Science* **2015**, *349*, 99−103.
(69) Quinn, C. M.; Wang, M.; Fritz, M. P.; Runge, B.; Ahn, J.; Xu, C.; Perilla, J. R.; Gronenborn, A. M.; Polenova, T. Dynamic Regulation of HIV-1 Capsid Interaction with the Restriction Factor TRIM5α Identified by magic-angle Spinning NMR and molecular dynamics Simulations. *Proc. Natl. Acad. Sci. U. S. A.* **2018**, *115*, 11519−11524.
(70) Wang, M.; Quinn, C. M.; Perilla, J. R.; Zhang, H.; Shirra, R., Jr.; Hou, G.; Byeon, I.-J.; Suiter, C. L.; Ablan, S.; Urano, E.; et al. Quenching Protein Dynamics Interferes with HIV Capsid Maturation. *Nat. Commun.* **2017**, *8*, 1779.
(71) Koning, R. I.; Gomez-Blanco, J.; Akopjana, I.; Vargas, J.; Kazaks, A.; Tars, K.; Carazo, J. M.; Koster, A. J. Asymmetric Cryo-EM Reconstruction of Phage MS2 Reveals Genome Structure In Situ. *Nat. Commun.* **2016**, *7*, 12524.
(72) Jaudzems, K.; Polenova, T.; Pintacuda, G.; Oschkinat, H.; Lesage, A. DNP NMR of biomolecular assemblies. *J. Struct. Biol.* **2019**, *206*, 90−98.
(73) Jung, J.; Byeon, I. J.; Ahn, J.; Concel, J.; Gronenborn, A. M. ^{1}H, ^{15}N and ^{13}C assignments of the Dimeric C-Terminal Domain of HIV-1 Capsid Protein. *Biomol. NMR Assignments* **2010**, *4*, 21−23.
(74) Hu, K. N.; Havlin, R. H.; Yau, W. M.; Tycko, R. Quantitative Determination of Site-Specific Conformational Distributions in an Unfolded Protein by Solid-State Nuclear Magnetic Resonance. *J. Mol. Biol.* **2009**, *392*, 1055−1073.
(75) Siemer, A. B.; Huang, K.-Y.; McDermott, A. E. Protein Linewidth and Solvent Dynamics in Frozen Solution NMR. *PLoS One* **2012**, *7*, No. e47242.
(76) Lange, S.; Linden, A. H.; Akbey, Ü.; Franks, W. T.; Loening, N. M.; van Rossum, B.-J.; Oschkinat, H. The Effect of Biradical Concentration on the Performance of DNP-MAS-NMR. *J. Magn. Reson.* **2012**, *216*, 209−212.
(77) Hu, K. N.; Yau, W. M.; Tycko, R. Detection of a Transient Intermediate in a Rapid Protein Folding Process by Solid-State Nuclear Magnetic Resonance. *J. Am. Chem. Soc.* **2010**, *132*, 24−25.
(78) Linden, A. H.; Lange, S.; Franks, W. T.; Akbey, Ü.; Specker, E.; van Rossum, B. J.; Oschkinat, H. Neurotoxin II Bound to Acetylcholine Receptors in Native Membranes Studied by Dynamic Nuclear Polarization NMR. *J. Am. Chem. Soc.* **2011**, *133*, 19266−19269.

DOI: 10.1021/acs.jpcb.9b02293
J. Phys. Chem. B 2019, 123, 5048−5058